Response to Reviewer 1 Queries/Comments

**Citation**: https://doi.org/10.5194/egusphere-2026-363-RC1

Dear Editor and Reviewer,

We appreciate you taking the time to provide us with all of your insightful and valuable comments and recommendations. All of them have been carefully considered, and we have made a concerted effort to answer them all in detail. Your unaltered original remarks are written in **grey** in this response, while our responses are written in **blue**. Certain key highlights in some of the responses have been emphasized using **bold text**.

**General Comments:**

Tiwari et al. derive the clear sky TOA direct radiative forcing due to black carbon (BCTOA DRF) using the outputs from the COSMO framework (their previous work) constrained by multi-spectral spaceborne AOD retrievals, and then employing SBDART model for BCTOA DRF calculation, for two geographical regions: Xuzhou and Dhaka. The BCTOA DRF estimated using SBDART is then used to train statistical ML model, whose efficacy is discussed in the manuscript for various microphysical properties (including amount) of BC. Shapley values were used to determine the contribution of different predictors in ML prediction of BCTOA DRF. The datasets used in this study, along with the methodology, are clearly described and well justified. The manuscript is well written and easy to follow. I have a few minor comments that aim to further improve the manuscript.

We sincerely thank the reviewer for the encouraging and constructive evaluation of our manuscript. We are grateful that the reviewer found the dataset selection, methodological framework, and scientific presentation to be clear, well justified, and easy to follow. In response to the comments, we made the following revisions to improve clarity, reproducibility, and figure presentation:

- **Methodological clarification:** Clarified how BC TOA DRF is calculated using COSMO-derived microphysical/optical properties and SBDART, added references for AOD–flux approaches, and specified the observational requirements for extending the framework to other AERONET/SONET sites.
- **ML-model transparency:** Defined the predictor variables, statistical metrics, Random Forest configuration, hyperparameters, and the rationale for comparing Linear, MLR, and ML models as a complexity gradient for BC TOA prediction.
- **Figure/text improvements:** Corrected figure labels, increased font sizes, reorganized crowded panels into the Supplement, added explicit panel references throughout the Results

We appreciate the comments provided, which have helped us improve the clarity, consistency, and presentation of the manuscript. All comments have been carefully considered and addressed in the revised version, as described in detail in the point-by-point responses below.

**Minor comments:**

Line 67: Are there any valid references which use linear AOD-flux relationship?

Thank you for this comment. We agree and have supported this statement with references at its first occurrence in the Introduction. Relevant examples of linear or radiative-efficiency-type AOD-TOA forcing approximations were cited in Section 2.2, where we discuss the linear surrogate model and the common practice of representing TOA forcing as a function of AOD. In the revised manuscript, we have now introduced these and additional references at Line 68.

The central idea in these approaches is that TOA shortwave flux or TOA aerosol forcing is empirically related to AOD, either through a regression between coincident satellite-retrieved AOD and TOA flux, or through a radiative-forcing-efficiency formulation in which the slope represents the TOA radiative response per unit aerosol loading. More recent examples like He et al. (2017) estimated TOA instantaneous aerosol direct radiative effects over the Yangtze River Basin using a linear relationship between CERES shortwave upward flux and coincident MODIS AOD550. Similarly, Biswas et al. (2017) estimated aerosol-free TOA flux over North-East India from a linear regression between CERES shortwave TOA fluxes and MODIS AOD, with the regression intercept representing the zero-AOD reference condition. These are directly adapted from Christopher and Zhang (2002) which used cloud-free, very low-AOD CERES-MODIS pixels to represent non-aerosol conditions when estimating shortwave aerosol radiative forcing over oceans. These examples support the statement that empirical AOD-flux or low-AOD reference approaches have been used in aerosol science community for aerosol forcing estimatation.

This is also why we include a linear benchmark model in our study: to evaluate how well traditional first-order BCAOD550-BCTOA approximation performs relative to the more physically informed MLR and ML models that include BC column loading and microphysical state.

Revised Manuscript text:

"*Furthermore, computing no-aerosol fluxes to derive net TOA forcing adds to the existing challenge. Studies often assume either linear AOD-flux relationships (computing* $TOA_{no\text{-}aerosol\text{-}flux}$ *at AOD =0) or using low-aerosol pixels for pristine flux (Biswas et al., 2017; Christopher and Zhang, 2002; Sundström et al., 2015).*"

Line 95: How is the BCTOA DRF calculated from TOA fluxes? The values reported in the results are strongly negative compared to the global mean low positive values reported in previous studies, also stated in lines 44 and 45 of the manuscript.

The adapted approach to compute BCDRF follows a sequence of: (a) observationally constrained optical property derivation, followed by (b) spatio-temporally hamonizing ancillary

datasets from multiple observation platrforms, and (c) simulation using these results and properties of (a) and (b) in the radative transfer model.

As discussed in the Introduction, estimating aerosol-type-specific forcing directly from satellite-observed TOA fluxes remains challenging because the observed flux contains the combined radiative influence of all aerosol species. Therefore, isolating the BC-specific contribution from observed TOA fluxes would require additional assumptions regarding aerosol composition, mixing state, vertical distribution, and the aerosol-free reference state.

In this study, we instead use an observation-constrained radiative transfer approach. First, we derive an ensemble of BC-containing aerosol microphysical states using the COSMO core–shell Mie framework. The BC core size and sulfate-shell size combinations are constrained by multi-waveband SSA from TROPOMI and AERONET/SONET, while accounting for cross-platform uncertainty and wavelength offsets. Only size/mixing-state combinations that reproduce the uncertainty-bounded SSA constraints across all wavelengths are retained. Second, these retained microphysical solutions are used to compute the aerosol optical properties required by the radiative transfer model. Specifically, BCAOD is calculated from the constrained core-shell size, particle density, extinction efficiency, mass extinction efficiency, and column mass density. The resulting BCAOD is then further screened using yet additional observational constraints: modeled BCAOD must remain below the observed total AOD upper bound at all of 388 nm, 470 nm, and 550 nm. Cases violating this column-feasibility condition at any wavelength are removed.

The final constrained aerosol optical properties, namely BCAOD, SSA, and ASY at 388, 470, and 550 nm, are then provided to SBDART together with satellite-derived ancillary inputs, including precipitable water vapour, surface spectral albedo, total column ozone, and model atmospheres varying month by month from ERA-5. The SBDART model then simulates both with and without aerosol fluxes thus computing net TOA forcing associated to BC.

The negative regional values reported in our results should therefore not be directly compared with the low positive global mean BC forcing values cited in the Introduction. Those literature values represent globally averaged BC forcing estimates. In contrast, our values are clear-sky, high-resolution, regional instantaneous TOA direct radiative effects over two heavily polluted urban agglomerations, computed for observation-constrained grid-days. In addition, our quantity represents the net TOA effect of BC-containing core-shell particles, where absorption by the BC core and scattering by the coating/column extinction act simultaneously. Under conditions of strong coating and high column extinction, scattering can dominate the TOA balance and yield negative TOA forcing, even while BC absorption contributes to atmospheric heating. This absorption-scattering competition is central to the regional behaviour discussed in the manuscript. Yet at the same time, the variability between the urban sites is based on real differences, since Xuzhou is controlled much more by secondary aerosol growth, while Dhaka is controlled much more by primary emissions as explained in Tiwari et al., 2025.

Line 112: Can this framework be expanded to other regions with AERONET stations, or are there any other special requirements?

Yes, the framework can in principle be expanded to other regions with AERONET, SONET, or equivalent sun-sky photometer stations. The framework requires a set of overlapping observational cosntraints and ancillary inputs. The key requirement is the availability of overlapping multi-platform constraints needed to retrieve BC-specific microphysics and column loading in a physically consistent way.

Specifically, this study wanted to include a broad spectrum covering UV-VIS-NIR, thus, the framework requires quality-controlled multi-waveband SSA from AERONET, SONET, or an equivalent sun-sky photometer network; satellite UV-SSA or absorption-related constraints; multi-waveband total AOD to impose column-feasibility filtering. Other anciallary inputs will strengthen the radiative transfer simulation.

The broader transferability of this deriving BC size and mixing state within a observationally cosntrained framework philosophy is supported by recent top-down BC studies. For example, Liu et al. (2024a) used OMI and AERONET observations with an inverse Mie framework to estimate BC mass and number column density on a day-by-day and grid-by-grid basis over South, Southeast, and East Asia. Similarly, Liu et al. (2024b) applied remotely sensed SSA as constraint from MISR satellite along with SONET to derive and diagnose changes in BC mass, number, size, and mixing state over Western China. In both cases RTM simulations were not carried out but size and mixing state of BC coated with non-absorbing shell were derived using obsevrational constraint using SSA information from OMI, MISR, AERONET and SONET in tandem. More recently, Liu et al. (2026) demonstrated that a multi-angle, multi-band satellite and Mie-scattering framework can be scaled globally to retrieve BC column concentration and microphysical information.

These studies support the transferability of the core retrieval concept, while the present study further extends it by adding a multi-waveband total-AOD feasibility constraint and coupling the constrained BC optical properties with SBDART for clear-sky BCTOA DRF estimation.

Line 210-220: Reference to your earlier work is missing here. Abbreviations MBE and MAE need to be defined. A brief note on the variables used to predict BCTOA, type of random forest model used along with the hyperparameters would be useful here.

Thank you for this helpful suggestion. We have now more clearly defined the predictor variables, statistical metrics, Random Forest configuration, and connection to the earlier COSMO-based retrieval work. We have revised Section 2.2 accordingly.

The predictors used to estimate BCTOA are the COSMO-derived and RTM-relevant variables: BCAOD550, aerosol column number density ($N_c$), aerosol column mass density ($M_c$), BC core size, and mixing state (defined as the ratio of BC core size to total particle size). These predictors are derived from the earlier observation-constrained COSMO framework described in in section 2.1.

We also now define the performance metrics at first use: mean bias error (MBE), mean absolute error (MAE), root mean square error (RMSE), and coefficient of determination ($R^2$). In addition, we have specified that the ML model is a Random Forest Regressor. The hyperparameters used were: n_estimators=100, max_depth=10, min_samples_split=5, min_samples_leaf=3, and max_features='sqrt'.

These settings were selected as a regularized configuration to balance predictive accuracy and generalization. Specifically, the number of trees provides a stable ensemble estimate, while the maximum tree depth and minimum split/leaf sizes limit overly deep trees and reduce overfitting. The use of 'sqrt' feature sampling decorrelates individual trees and improves ensemble robustness. The suitability of this configuration is supported by the close agreement between training and independent test performance, near-zero MBE, high $R^2$, and the 5-fold cross-validation results reported in the Supplement Figure S1. The manuscript has been revised to include these details.

Revised manuscript text:

*"Specifically, we used a Random Forest Regressor to predict COSMO-RTM derived BCTOA from the COSMO-derived predictor variables. The predictors were BCAOD550, aerosol column number density ($N_C$), aerosol column mass density ($M_C$), BC core size, and mixing state (defined as the ratio of BC core size to total particle size). These variables are derived from the observation-constrained COSMO retrieval framework described in Section 2.1. For each region's RTM output BC TOA is subjected to a 70-30 train-test split, with 70% of the data used to train the model and 30% withheld as an independent test set. This approach allowed the model to learn relationships between predictors and BC TOA while ensuring a robust evaluation on unseen data. The Random Forest hyperparameters were set as follows: n_estimators=100, max_depth=10, min_samples_split=5, min_samples_leaf=3, and max_features='sqrt'. These regularized settings were used to provide a stable ensemble prediction while limiting overfitting through restricted tree depth, minimum node sizes, and randomized feature selection.*

*The statistical metrics (coefficient of determination ($R^2$), mean bias error (MBE), mean absolute error (MAE) and root mean square error (RMSE)) for both the training and test data are presented, along with the corresponding predicted vs. actual plots for each set along with their statistics and error metrics provided in Supplement Figure S1 and Supplement Table S1 respectively."*

Figure 3: Bottom panels are not correctly labelled. Also, the font size is too small for the last two panels in bottom row and should be increased.

Thank you for this helpful comment. We have revised Figure 3 to correct the bottom-panel labels and improve figure readability. The font sizes of the subplot titles, axis labels, tick labels, and legends have been increased throughout, with particular attention to the bottom-row panels.

We have also reorganized the bottom panels for clarity. The former small 2D core-shell KDE panels, previously shown as panels h and i, have been removed from the main figure, enlarged, and combined into a separate supplementary figure as Supplement Fig. S3. The revised Figure 3 now focuses on the one-dimensional probability density distributions of the key BC-related parameters, including the polluted-condition core-to-shell ratio, polluted-condition BC core size, and the $BCAOD_{550}$ distribution under small-core conditions.

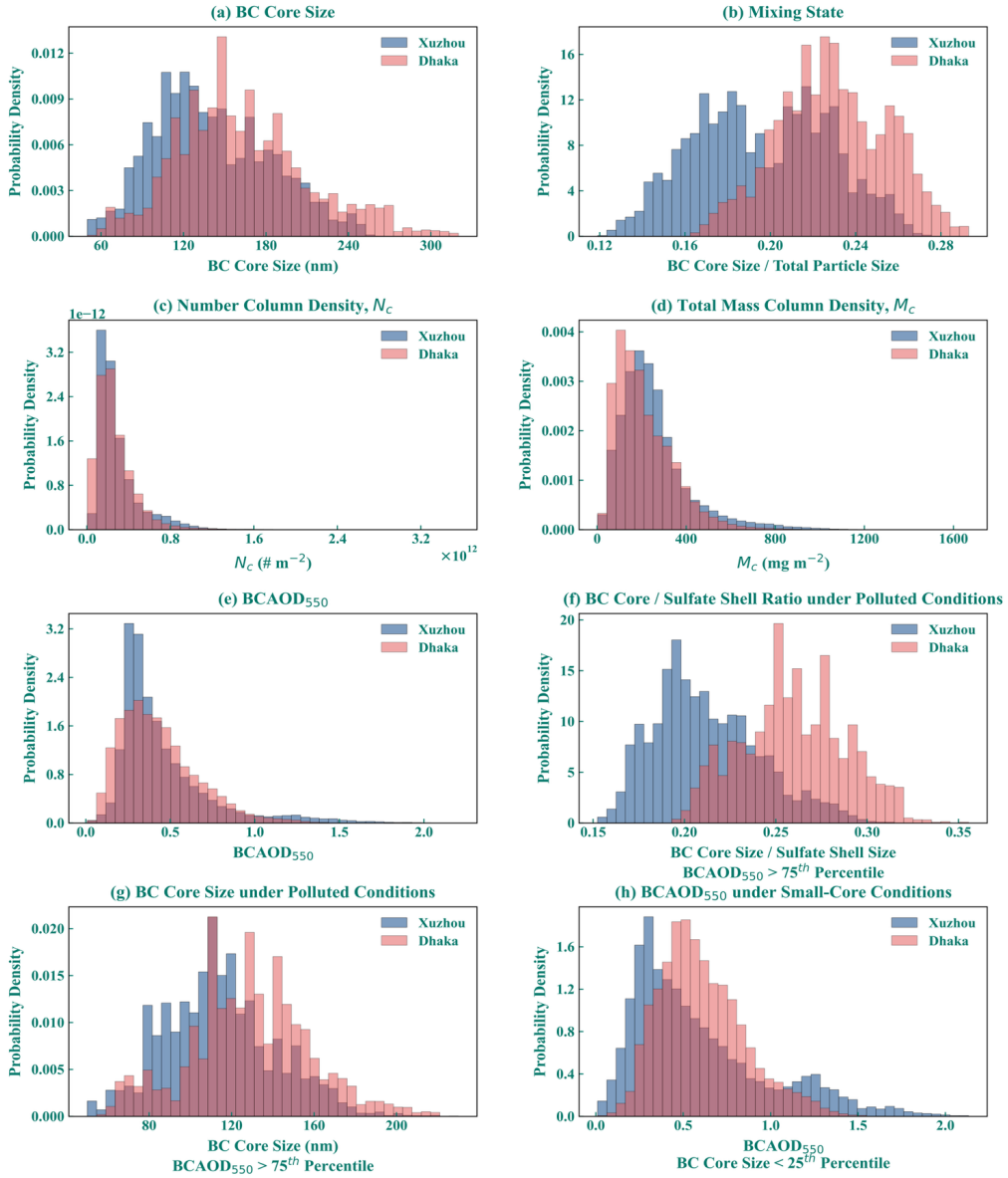


**Figure 3: Probability density distributions of key predictors for aerosol radiative forcing analysis in Xuzhou and Dhaka: a.) Black Carbon (BC) core size, b.) Mixing state (ratio of BC size to total size), c.) Number column density ($N_c$), d.) Total mass column density ($M_c$), and e.) BCAOD at 550 nm, f.) BC core to Sulfate shell size ratio ($BCAOD_{550}$>75$^{th}$ percentile), g.) BC core size for polluted**

**condition ($BCAOD_{550}$>75$^{th}$ percentile), h.) $BCAOD_{550}$ distribution (BC core size < 25$^{th}$ Percentile or under barely coated conditions)**

**Supplement Figure S3.**

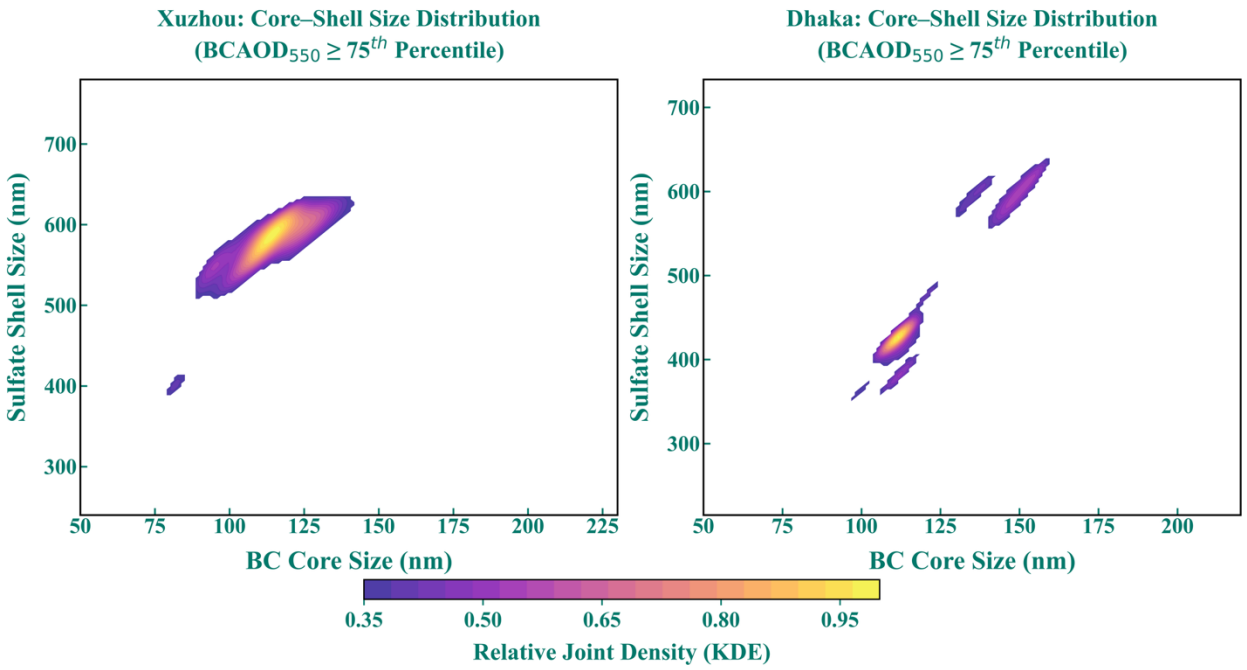


**Supplement Figure S3. Dominant BC core-sulfate shell size distributions under polluted conditions ($BCAOD_{550}$ >75$^{th}$ percentile in Xuzhou and Dhaka. Color shading shows the relative joint KDE density normalized by the regional maximum, indicating the most frequent core–shell microphysical states during high-loading conditions.**

Lines 280-335: While the values of the different BC-related parameters are taken from Figure 3, it would improve clarity if the corresponding panels (a–i) are explicitly referenced when these parameters are discussed.

In addition, we have revised the corresponding text in Lines 280–335 to explicitly reference the relevant Figure 3 panels when each parameter is discussed. The general BC microphysical and loading distributions are now linked to Fig. 3 (a-e), the polluted-condition core-to-shell ratio and BC core size distributions are linked to Fig. 3 (f,g), and the small-core BCAOD550 distribution is linked to Fig. 3 (h).

Section 3.2: The rationale for comparing different statistical models for predicting BCTOA is not stated in the manuscript. If the authors wanted to show the benefit of using a random-forest model compared to multi-linear regression or linear regression, they could just state the additional information in the supplementary or appendix. Adding a separate section for this

comparison seems unnecessary and I suggest moving this section to supplementary and briefly stating the benefit of using ML-based model in the main text.

We thank the reviewer for highlighting this, and we take this as an opportunity to better articulate the scientific value of this comparison, which goes beyond a methodological benchmarking exercise, since we do agree with the comment that from a purely methodological perspective it makes sense to move this to the appendix.

The rationale for comparing the three surrogate models is established in Section 2.2, where we note that the atmospheric science community still commonly adopts a linear radiative efficiency approach by assuming TOA forcing scales linearly with AOD - a widespread simplification, that "**overlooks non-linear modulations in TOA forcing caused by microphysical variability, column number loading, and their role in both absorption and extinction efficiency**." The three models are designed precisely to test this hierarchy of complexity based on the current trends following the atmospheric radiative forcing community: the linear model mimicking community practice, the MLR model expanding to additional predictors while retaining linearity, and the random forest model capturing nonlinear interactions. We acknowledge, however, that this connection between Section 2.2 and Section 3.2 could have been stated more explicitly, and we add a brief bridging paragraph at the opening of Section 3.2 to make this clearer.

Beyond model comparison, Section 3.2 serves three interconnected scientific purposes that we feel warrant its retention in the main text:

**First,** it quantifies the real-world cost of the linear approximation across diverse pollution and microphysical regimes. The finding that the linear model fails entirely under barely-coated BC conditions in Xuzhou (Adj. $R^2$ = -0.20) and degrades severely for very large BC cores (MAPE = 38.6%) is a physically meaningful result that directly supports the paper's central argument that simplified BC forcing parameterizations are inadequate.

**Second,** it reveals the transition-regime problem, where models including ML exhibit reduced variance explanation despite low absolute errors in mid-range TOA categories. This bias-variance trade-off is not a routine modeling artifact - it reflects the complex, competing absorption-scattering dynamics that govern the crossover between cooling and warming regimes, which directly motivates the SHAP analysis presented in Section 3.3. Relocating Section 3.2 to supplementary material would therefore sever this narrative connection.

**Third,** the regime-stratified performance analysis across coating thickness and BC core size categories provides physical insight into which atmospheric conditions pose the greatest challenge for simplified approaches, reinforcing the paper's conclusion that no universal BC forcing parameterization is currently feasible.

We therefore propose retaining Section 3.2 in the main text, with the addition of a bridging paragraph that more explicitly connects the motivation established in Section 2.2 to the results that follow. We are happy to further revise if the reviewer feels additional changes are needed.

In the revised manuscript, we have added the following sentences at the opening of Section 3.2 to better articulate the scientific rationale for this comparison:

"*As outlined in Section 2.2, the three surrogate models span a deliberate complexity gradient, from AOD-only linear scaling, to multivariate parametric regression, and ultimately nonlinear ensemble learning, with each model tier designed to probe a distinct aspect of BC-radiation interaction. Their performance is assessed both in aggregate and across distinct pollution, coating, and size regimes, where the physical drivers of BC TOA forcing are expected to differ most.*"

Section 3.2: please refer to specific panels in Figure 4 appropriately while discussing them in the text.

We thank the reviewer for this observation. Specific panel references have been added in Section 3.2, with scatter density comparisons referenced as Figures 4a-c for Xuzhou and Figures 4d–f for Dhaka. Percentile-based distributional comparisons are now referenced to Supplementary Figure S4, which shows the PDF plots relocated from the original Figure 4.

Figures 4 and 6: Axis labels are hard to read. Please increase their font size.

We thank the reviewer for this observation. In the revised manuscript, Figure 4 has been reorganized to address concerns raised by regarding figure crowding. Specifically, the PDF comparison plots between the surrogate models and SBDART BCTOA have been relocated to Supplementary Figure S4, allowing Figure 4 to focus solely on the scatter density plots for Xuzhou (Figures 4a-c) and Dhaka (Figures 4d-f). This reorganization also allowed us to increase the font sizes of axis labels, tick marks, and legend text throughout Figure 4 to improve readability.

The revised Figure 4 is shown below for convinience:

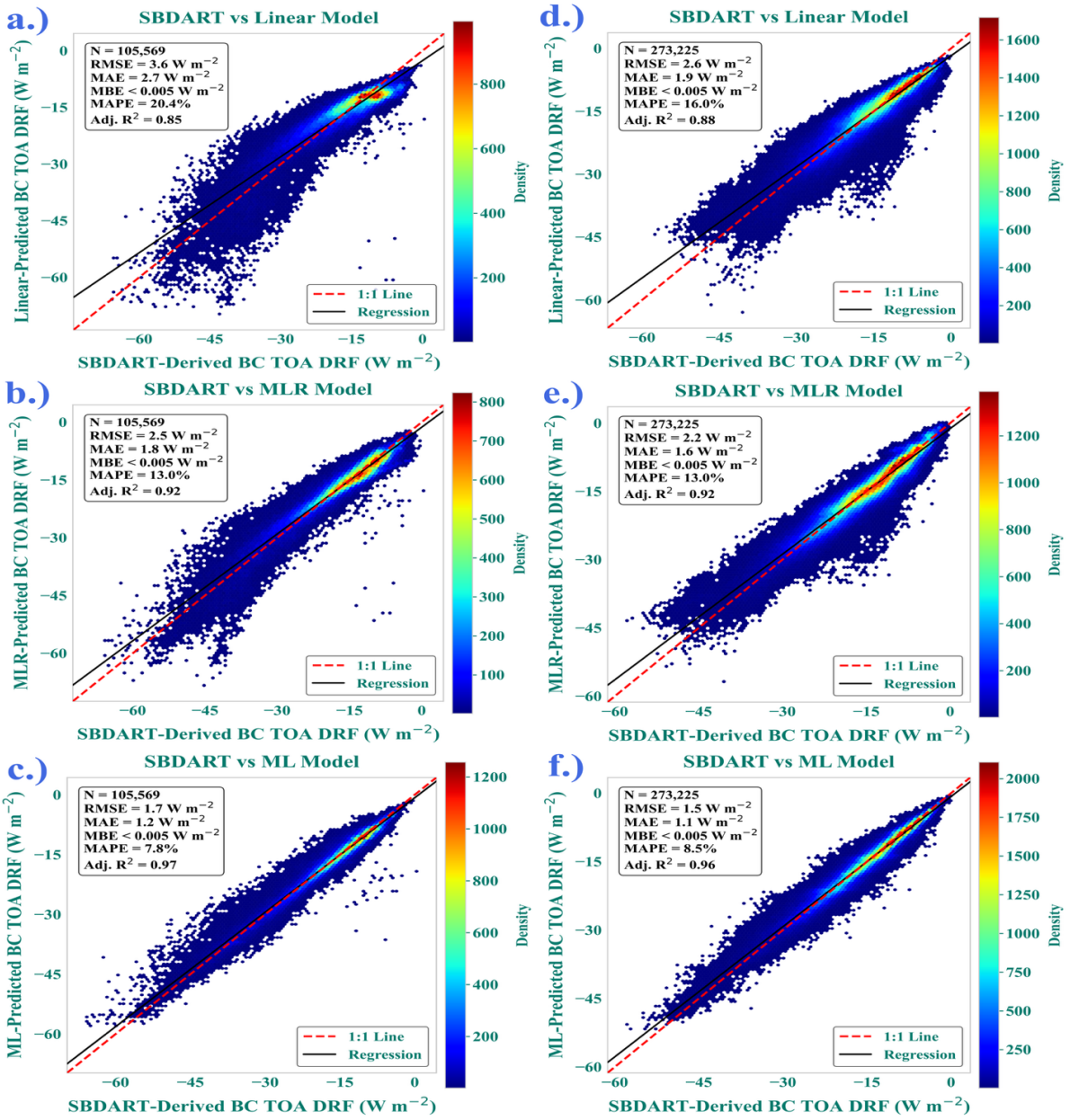


**Figure 4: Comparison of BCTOA predictions from various models (Linear, MLR, and ML) with SBDART TOA for Xuzhou (a-c) and Dhaka (d-f). The scatter plots (top row) display the relationship between model predictions and SBDART values, with color maps indicating the density of data points.**

The PDF plots have now been replotted and moved in to the Supplement Figure S3:

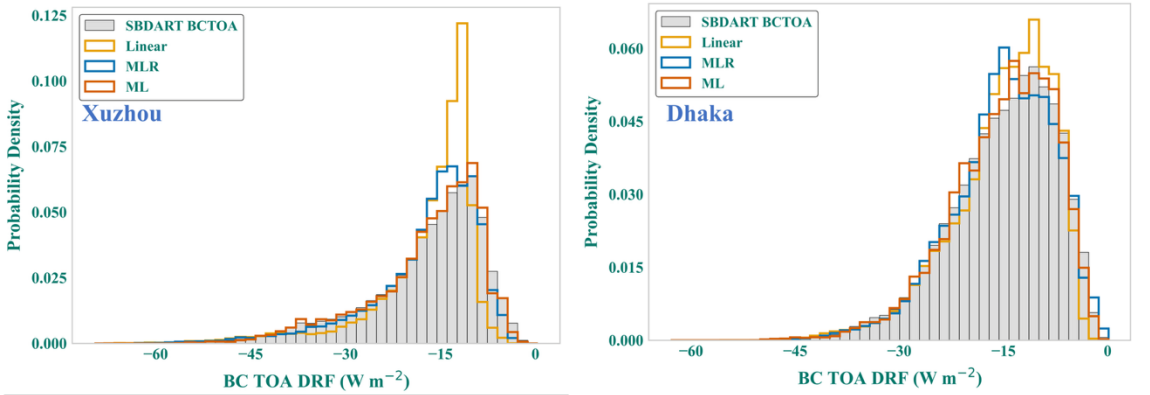


| Percentile | SBDART | Linear | MLR | ML |
|---|---|---|---|---|
| 1st | -45.4 | -49.0 | -47.9 | -43.9 |
| 99th | -4.1 | -7.2 | -5.1 | -4.5 |

| Percentile | SBDART | Linear | MLR | ML |
|---|---|---|---|---|
| 1st | -37.1 | -37.6 | -36.5 | -36.5 |
| 99th | -2.8 | -4.4 | -2.2 | -3.1 |

**Figure S4: Probability density functions (PDFs) of BCTOA values from SBDART and the three surrogate models (Linear, MLR, and ML) for Xuzhou (left) and Dhaka (right). Tabulated percentile values at the 1st and 99th percentiles are provided below each panel to compare the distributional extremes.**

Similarly, for Figure 6 we have revised and re-organized the plot for clarity as shown below:

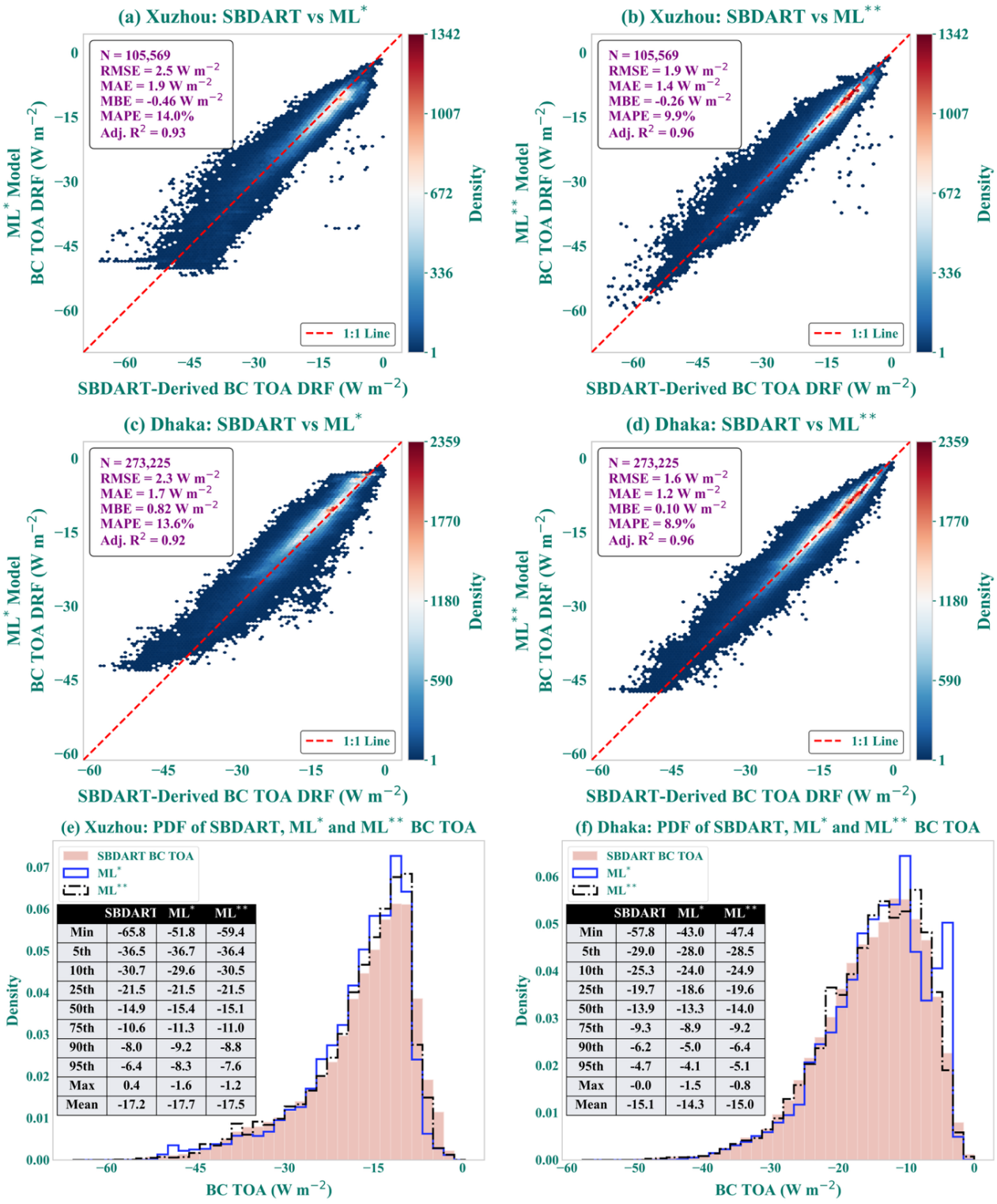


**Figure 6: Comparison of SBDART-derived BCTOA forcing with cross-regional (ML*) and combined (ML**) ensemble learning models for Xuzhou (a-b) and Dhaka (c-d). PDF comparisons**

**between SBDART BCTOA and ML-predicted BCTOA, with statistical summaries of BCTOA distributions at different percentiles (e-f).**

Line 392: By "environmental" do you mean different source regions?

We thank the reviewer for this observation. Then intention was to compare performance of models across different in-situ microphysical conditions of coating thickness and core size, attempting to account for atmospheric aging, oxidant availability, and emission characteristics. We acknowledge the term is may seem out of place or ambiguous here since Table 1 strictly stratifies specifically by microphysical regimes. We have revised the sentence to:

*"To assess model performance under different microphysical conditions, performance metrics are compared across distinct mixing state and BC core size regimes and tabulated in Table 1."*

Lines 455-465: Please correct repeated information.

We thank the reviewer for this observation. The repeated reference to *Tiwari et al., (2023)* and the reiteration of the scattering-absorption argument in Lines 455-465 have been removed and consolidated into a single concise statement in the revised manuscript. The revised manuscript now reads:

"*This microphysics-driven TOA sign variability, previously demonstrated by Tiwari et al., (2023), likely arises from non-linear changes in absorption, scattering and scattering angle that occur simultaneously with small changes in the mixing ratio and core size in tandem. While such interactions and sensitivity are often high AOD contributing to more negative TOA forcing is consistent with the total attenuation under the conditions where scattering enhancement is larger than the absorption enhancement.*"

Line 536: Please include the number of years of data that was used in generating the "regional climatology" shown in Figure 7?

The spatial maps in Figure 7 represent pixel-by-pixel weighted averages computed across all available clear-sky observation days spanning April 2018 to April 2022. Accordingly we have revised the caption of Figure 7.

Figures 7 and 8: What geographical radius was used for estimating BC TOA DRF around each AERONET station? How were this radius chosen?

We thank the reviewer for this question. The spatial maps in Figures 7 and 8 were generated over a 150 km radius Haversine circle centered on the AERONET station in each region (Xuzhou_CUMT for Xuzhou; Dhaka_University for Dhaka).

The 150 km radius was chosen based on several considerations. First, under typical strong wind conditions of ~5 m/s, air parcels would require many hours to traverse 150 km, meaning absorbing aerosol properties observed at the AERONET station on a given day remain physically

representative within this distance. Second, existing literature supports AERONET's spatial representativeness extending up to 200–400 km under stable aerosol conditions (Fu et al., 2018; Mishra et al., 2016), making 150 km a conservative and defensible choice. Third, this radius avoids the overly broad assumptions of a 2° × 2° grid representativeness that may dilute regional detail, while also avoiding finer scales that risk losing broader spatial coherence essential for regional characterization (Wang et al., 2018; Schutgens, 2020).

Critically, the 150 km radius is used only to define the spatial domain over which BC microphysical type - constrained through multi-waveband SSA consistency is assumed representative. Column loading quantities such as mass and number density are derived independently for each valid pixel based on actual satellite observations, with no spatial homogeneity assumption applied to aerosol abundance.

In summary, the 150 km radius represents a balanced and physically motivated choice that preserves both spatial relevance and regional coherence. It is conservative enough to maintain optical consistency across retained pixels while being broad enough to capture the regional aerosol environment characteristic of each urban agglomeration.

We acknowledge that as denser observational networks and higher resolution geostationary data become available, these spatial boundaries can be further refined to better capture fine-scale aerosol heterogeneity within and around these regions.

**References:**


Biswas, J., Pathak, B., Patadia, F., Bhuyan, P. K., Gogoi, M. M., & Babu, S. S. (2017). Satellite-retrieved direct radiative forcing of aerosols over North-East India and adjoining areas: climatology and impact assessment. *International Journal of Climatology*, *37*(13), 4756. https://doi.org/10.1002/joc.5325

Christopher, S. A., & Zhang, J. (2002). Shortwave Aerosol Radiative Forcing from MODIS and CERES observations over the oceans. *Geophysical Research Letters*, *29*(18). https://doi.org/10.1029/2002gl014803

Fu, D., Xia, X., Wang, J., Zhang, X., Li, X., & Liu, J. (2018). Synergy of AERONET and MODIS AOD products in the estimation of PM2.5 concentrations in Beijing. *Scientific Reports*, *8*(1), 10174. https://doi.org/10.1038/s41598-018-28535-2

He, L., Wang, L., Lin, A., Zhang, M., Bilal, M., & Tao, M. (2017). Aerosol Optical Properties and Associated Direct Radiative Forcing over the Yangtze River Basin during 2001–2015. *Remote Sensing*, *9*(7), 746. https://doi.org/10.3390/rs9070746

Liu, J., Cohen, J. B., Tiwari, P., Liu, Z., Yim, S. H., Gupta, P., & Qin, K. (2024a). New top-down estimation of daily mass and number column density of black carbon driven by OMI and AERONET observations. *Remote Sensing of Environment*, *315*, 114436. https://doi.org/10.1016/j.rse.2024.114436

Liu, Z., Cohen, J. B., Tiwari, P., Guan, L., Wang, S., Li, Z., & Qin, K. (2026). A global black carbon dataset of column concentration and microphysical information derived from MISR multi-band observations and Mie scattering simulations. *Earth System Science Data*, *18*(1), 507–533. https://doi.org/10.5194/essd-18-507-2026

Liu, Z., Cohen, J. B., Wang, S., Wang, X., Tiwari, P., & Qin, K. (2024b). Remotely sensed BC columns over rapidly changing Western China show significant decreases in mass and inconsistent changes in number, size, and mixing properties due to policy actions. *Npj Climate and Atmospheric Science*, *7*(1). https://doi.org/10.1038/s41612-024-00663-9

Mishra, A. K., Rudich, Y., & Koren, I. (2016). Spatial boundaries of Aerosol Robotic Network observations over the Mediterranean basin. *Geophysical Research Letters*, *43*(5), 2259–2266. https://doi.org/10.1002/2015gl067630
Schutgens, N. a. J. (2020). Site representativity of AERONET and GAW remotely sensed aerosol optical thickness and absorbing aerosol optical thickness observations. *Atmospheric Chemistry and Physics*, *20*(12), 7473–7488. https://doi.org/10.5194/acp-20-7473-2020

Sundström, A., Arola, A., Kolmonen, P., Xue, Y., De Leeuw, G., & Kulmala, M. (2015). On the use of a satellite remote-sensing-based approach for determining aerosol direct radiative effect over land: a case study over China. *Atmospheric Chemistry and Physics*, *15*(1), 505–518. https://doi.org/10.5194/acp-15-505-2015

Tiwari, P., Cohen, J. B., Lu, L., Wang, S., Li, X., Guan, L., Liu, Z., Li, Z., & Qin, K. (2025). Multi-platform observations and constraints reveal overlooked urban sources of black carbon in Xuzhou and Dhaka. *Communications Earth & Environment*, *6*(1). https://doi.org/10.1038/s43247-025-02012-x

Wang, R., Andrews, E., Balkanski, Y., Boucher, O., Myhre, G., Samset, B. H., Schulz, M., Schuster, G. L., Valari, M., & Tao, S. (2018). Spatial representativeness error in the Ground-Level observation networks for black carbon radiation absorption. *Geophysical Research Letters*, *45*(4), 2106–2114. https://doi.org/10.1002/2017gl076817